iScience

CellPress

Article

Adaptive Regulation of Nitrate Transceptor NRT1.1 in Fluctuating Soil Nitrate Conditions

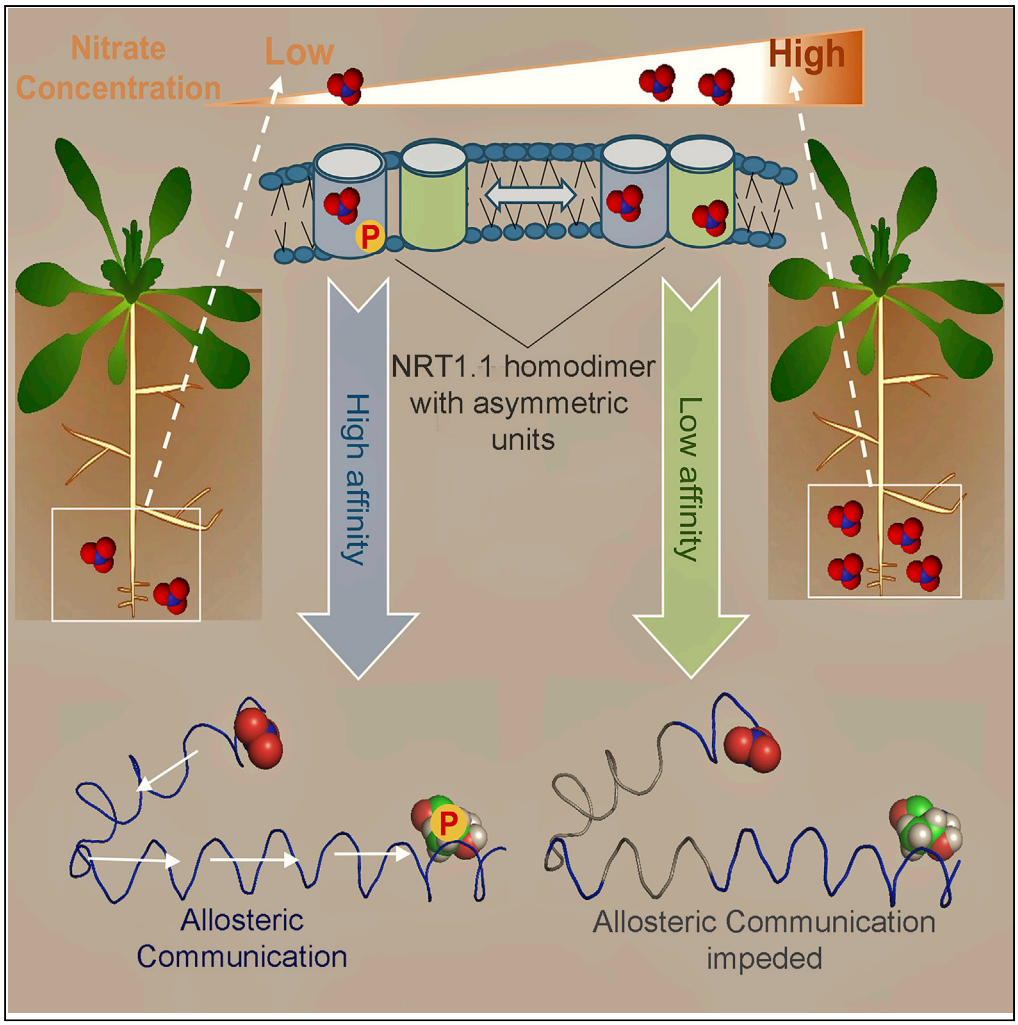

Mubasher Rashid, Soumen Bera, Alexander B. Medvinsky, Gui-Quan Sun, Bai-Lian Li, Amit Chakraborty

amitc.maths@curaj.ac.in

HIGHLIGHTS

NRT1.1 interprotomer asymmetry provides a functional basis for dual affinity

Nitrate-triggered conformational changes facilitate intraprotomer allostery

NRT1.1 interprotomer asymmetry is correlated with the phosphorylation switch

Allostery plays a critical role in regulating the phosphorylation

Rashid et al., iScience 2, 41–50
April 27, 2018
https://doi.org/10.1016/j.isci.2018.03.007

iScience

CellPress

Article

Adaptive Regulation of Nitrate Transceptor NRT1.1 in Fluctuating Soil Nitrate Conditions

Mubasher Rashid,[1] Soumen Bera,[1] Alexander B. Medvinsky,[2] Gui-Quan Sun,[3] Bai-Lian Li,[4] and Amit Chakraborty[1,4,5,*]

SUMMARY

Plant adaptation in variable soil nitrate concentrations involves sophisticated signaling and transport systems that modulate a variety of physiological and developmental responses. However, we know very little about their molecular mechanisms. It has recently been reported that many of these responses are regulated by a transceptor NRT1.1, a transporter cum receptor of nitrate signaling. NRT1.1 displays dual-affinity modes of nitrate binding and establishes phosphorylated/non-phosphorylated states at the amino acid residue threonine 101 in response to fluctuating nitrate concentrations. Here we report that intrinsic structural asymmetries between the protomers of the homodimer NRT1.1 provide a functional basis for having dual-affinity modes of nitrate binding and play a pivotal role for the phosphorylation switch. Nitrate-triggered local conformational changes facilitate allosteric communications between the nitrate binding and the phosphorylation site in one protomer, but such communications are impeded in the other. Structural analysis therefore suggests the functional relevance of NRT1.1 interprotomer asymmetries.

INTRODUCTION

Nitrate is an essential mineral nutrient in plants and at the same time acts as a signaling molecule (Crawford, 1995; Wang et al., 2004). Its soil concentrations, however, fluctuate in several orders of magnitude from micromolar to millimolar range. To cope with these fluctuations, plants have developed sophisticated sensing and transport systems (Krouk et al., 2010). Rigorous molecular studies on ammonium and nitrate uptake have demonstrated the existence and functioning of two distinct uptake systems in plants referred to as high-affinity transport system (HATS) and low-affinity transport system (LATS) (Crawford and Glass, 1998; von Wirén et al., 2000). In low nutrient concentration, HATS is ON to scavenge ions and allows plants to maintain a normal uptake rate (Liu and Tsay, 2003; Nacry et al., 2013). In high nutrient concentration, LATS is ON, leading to increased uptake along increasing nitrate gradient (Wang et al., 1993; Nacry et al., 2013). HATS usually follows Michaelis-Menten kinetics and displays saturation characteristics relative to LATS that increase linearly with concentrations. These differences primarily indicate the involvement of distinct sets of genes. Indeed, there are two distinct families of nitrate transporter genes, NRT1 and NRT2, associated with LATS and HATS, respectively (Williams and Miller, 2001). With an interesting exception, recent studies have revealed that the nitrate transporter NRT1.1 (also known as NPF6.3 or CHL1), which is distinct from most of the members of both HATS and LATS gene family, contributes to both the systems and functions as *transceptor* (Ho et al., 2009; Giehl and von Wirén, 2015), a transporter cum receptor of changes in soil nitrate concentration. The dual-affinity modes of nitrate binding (Liu et al., 1999) and a phosphorylation switch allows NRT1.1 protein to control its capacity of switching between high- and low-affinity modes of uptake (Tsay, 2014). Detailed understanding of this molecular mechanism is essential for improving plant nutrient use efficiency (NUE) (Good et al., 2004; Gutierrez et al., 2012) in a wide range of variation in soil nutrient availabilities, which, however, remains largely unknown.

Independent of its transporter function, NRT1.1 also acts as a nitrate sensor, leading to rapid transcriptional regulations of several transporters and assimilatory genes called primary nitrate response (PNR) (Krouk et al., 2006; Ho et al., 2009). In the face of a wide range of variation in extracellular nitrate availabilities, plant adaptation is accompanied by quantifiable changes in PNR mediated by NRT1.1. *In vitro* and *in vivo* studies showed a biphasic primary response; at low nitrate concentrations, protein kinase CIPK23 phosphorylates Thr101 of NRT1.1, which allows the maintenance of a low-level primary response relative to the PNR level at high nitrate concentration (Ho et al., 2009). PNR studies in transgenic plants suggest that dual-affinity binding of nitrate and phosphorylation switch jointly allow NRT1.1 to sense a wide range of extracellular nitrate availabilities and are mainly responsible for biphasic adjustment of

[1]School of Mathematics, Statistics and Computational Sciences, Central University of Rajasthan, Bandarsindri, Ajmer, India

[2]Institute of Theoretical and Experimental Biophysics, Pushchino 142290, Russia

[3]Department of Mathematics, Shanxi University, Taiyuan, People's Republic of China

[4]Department of Botany and Plant Sciences, University of California, Riverside, USA

[5]Lead Contact

*Correspondence: amitc.maths@curaj.ac.in

https://doi.org/10.1016/j.isci.2018.03.007

PNR (Medici and Krouk, 2014; Krouk, 2017). In *nrt1.1* loss-of-function mutant plant *Arabidopsis thaliana*, it has evidently been noted that NRT1.1 regulates the expressions of the dedicated high-affinity transporter *nrt2.1*. At high nitrate concentrations, the expression of *nrt2.1* is not down-regulated when *nrt1.1* function is lost, which indicates a critical role of NRT1.1 in the PNR (Bouguyon et al., 2015). However, it remains unknown how the biphasic states of the PNR are regulated by sensing extracellular availabilities of nitrate concentrations.

A key question about the biphasic states of NRT1.1 and their connection with dual-affinity nitrate binding and the phosphorylation at Thr101 has a potential structural basis. Recently reported apo- and nitrate-bound crystal structures of *Arabidopsis thaliana* NRT1.1 revealed a critical role of His 356 in nitrate binding and a phosphorylation-controlled dimerization switch that allows NRT1.1 to retain a dual-affinity mode of nitrate uptake (Sun et al., 2014; Parker and Newstead, 2014). This suggests that assembly and disassembly of the homodimer NRT1.1 controlled by the phosphorylation is responsible for toggling between low- and high-affinity modes of nitrate uptake (Sun et al., 2014). Despite this significant structural analysis, questions remain as to how the post-translational modifications associated with the nitrate sensing enables NRT1.1 to cope with a wide range of nitrate fluctuations. By comparative structural analyses of apo- and nitrate-bound X-ray crystallographic data of *Arabidopsis thaliana* NRT1.1 (Parker and Newstead, 2014), we report here that the intrinsic local asymmetries between the two protomers of NRT1.1 around the binding and Thr101 sites that are further enhanced by the nitrate binding provide a functional basis for having dual-affinity modes of nitrate binding. These asymmetries poise both the protomers for differential allosteric communications between the binding and phosphorylation sites, thereby regulating the phosphorylation-controlled dimerization of NRT1.1.

RESULTS

Interprotomer Asymmetries and Differential Nitrate-Binding Affinities

To examine dual-affinity nitrate binding, comparative analyses were carried out between apo- and nitrate-bound crystal structures of *Arabidopsis thaliana* NRT1.1. The transporter protein NRT1.1 is a 590-amino-acid homodimer consisting of two asymmetric inward-facing units, protomer A and protomer B. While viewed from the side, the nitrate transporting tunnels in both the protomers are not in parallel but tilted at ~15° angles with the central two-fold axis in opposite direction (Sun et al., 2014). Relative positions of the nitrate to its surrounding residues within the distance of 4.0 Å differ between the monomers. In the apo-protein, the protomer A nitrate-binding pocket consists of the residues Leu 49, His 356, Leu 359, Thr 360, Tyr 388, and Phe 511, with the minimum distances of 3.0 and 2.0 Å between the central nitrate atom and His 356 and Thr 360, respectively. However, the protomer B nitrate-binding pocket consists of Arg 45, Thr 48, Leu 49, Phe 82, and His 356, with minimum distances of 4.0 and 3.7 Å from the central nitrate atom to Arg 45 and His 356, respectively. Compared with the apo-protein structure, the nitrate-bound NRT1.1 protomer A neighborhood composition differs by the residues Val 53 and Leu 78, and in protomer B the composition differs by the residues Leu 78, Thr 360, and Phe 511 (Table S1, Figure S1). It is further noted that nitrate binds to Thr 360 and His 356 through H-bonding in protomer A, whereas in protomer B Thr 360 is replaced by Arg 45 (Figure S2). As observed by Parker and Newstead, (2014), the presence of His 356 in both the protomers seems to be necessary for nitrate binding following its protonation. Mutation of only His 356 has resulted in complete loss of nitrate binding.

The phosphorylation site Thr101 is entirely buried in a hydrophobic pocket surrounded by the residues Gly 88,97,162; Ile 91,102,104; Ala 92,103; Phe 105; Leu 100 within 4.0 Å neighborhood of apo-protein protomer A. In contrast, the Thr 101 site in protomer B is surrounded by the additional residues Ala 106, 165 and Val 163 within the same neighborhood. In the nitrate-bounded structure, the Thr101 neighborhood composition in protomer A consists of additional residues Ala 106 and Val 163, whereas protomer B consists of additional residues Ala 165 with respect to the apo-structure. Ramachandran plot clearly shows significant conformational changes of both the nitrate-binding residues and phosphorylation sites Thr 101 located at the region of the right-handed helix (Figure 1, Table S2). Moreover, in the interface of the apo-structure with the interfacing area A.1093 $Å^2$ and B.1099 $Å^2$, besides the non-bonded contacts, the only bonded contacts present are four hydrogen bonds: A.Thr111–B.Val229, A.Thr111–B.Ser233, A.Thr111–B.Ser233, A.Val229–B.Thr11. After nitrate binding, all the four interactions are completely lost with reduced interfacing surface area, and a single new H-bond is built between A.Ser233 and B.Thr111 (Table S3). This analysis therefore indicates nitrate-triggered local conformational changes, enhancing asymmetries between the protomers.

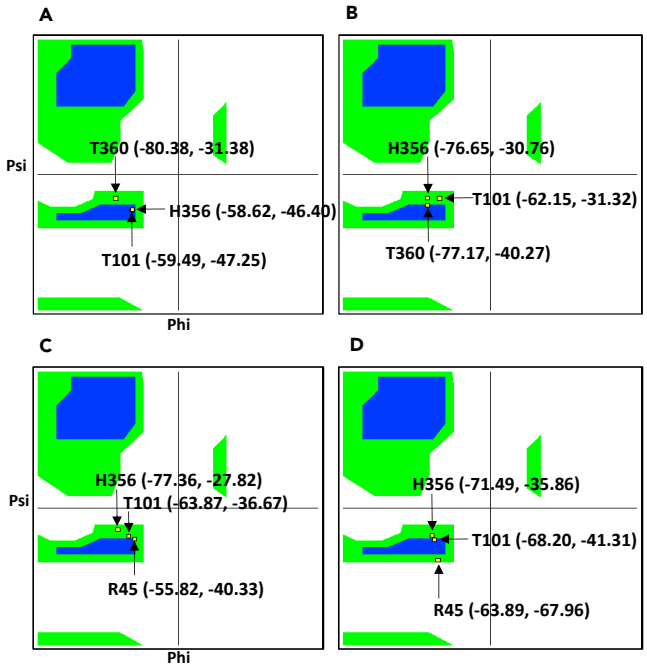

Figure 1. Ramachandran Plots Showing Differences in Phi and Psi Angles before and after Nitrate Binding

(A) Protomer A nitrate unbounded; (B) protomer A nitrate bounded. In (A) and (B), H356 and T360 are the ligand-binding pocket residues and T101 is the phosphorylation site. (C) Protomer B nitrate unbounded; (D) protomer B nitrate bounded. In (C) and (D), H356 and R45 are the binding pocket residues.

The observed interprotomer local conformational asymmetry is corroborated by the residual electron density within the 4.0-Å neighborhood of the nitrate-binding site and the phosphorylation site Thr 101 (Figure 2). The $2F_{obs} - F_{calc}$ electron density maps contoured at 2.0 sigma, representing local conformational asymmetries, are calculated for the apo- (Figure S3) and nitrate-bounded (Figure 2) NRT1.1 crystals. To correlate this intrinsic asymmetry with the nitrate-bounded states, differences between backbone chemical shifts, $^{13}C\alpha$ $\Delta\delta$, of protomers A and B are predicted with SHIFTX2 (Han et al., 2011) (Figure 3A), which combines ensemble machine learning methods with sequence alignment-based methods. It shows a wide range of variation of $\Delta\delta$ in both protomers A (0.003–3.6 ppm) and B (0.003–4.0 ppm). Several

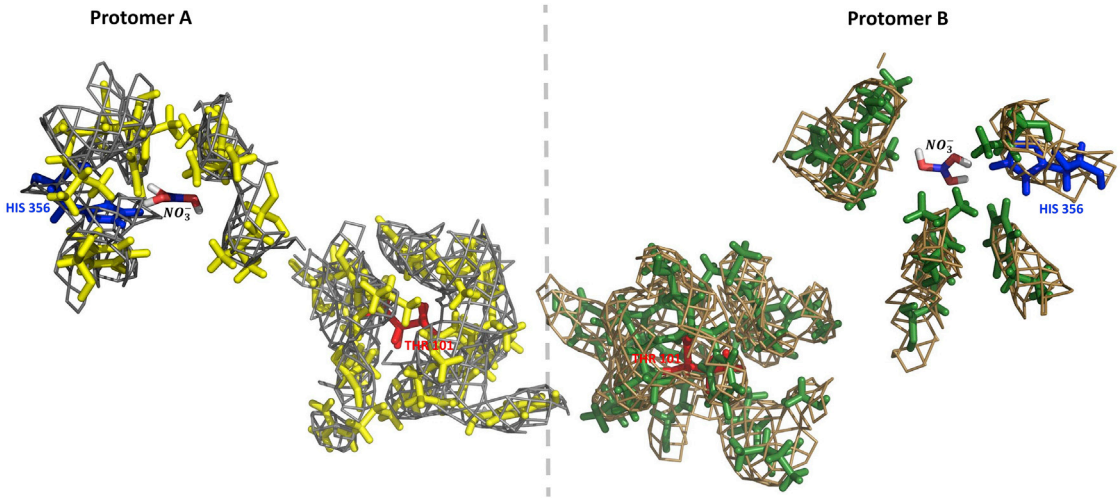

Figure 2. $2F_{obs} - F_{calc}$ Electron Density Maps Contoured at 2.0σ

It represents local conformational asymmetries, which are calculated for the nitrate-bounded NRT1.1 crystals (PDB: 5a2o).

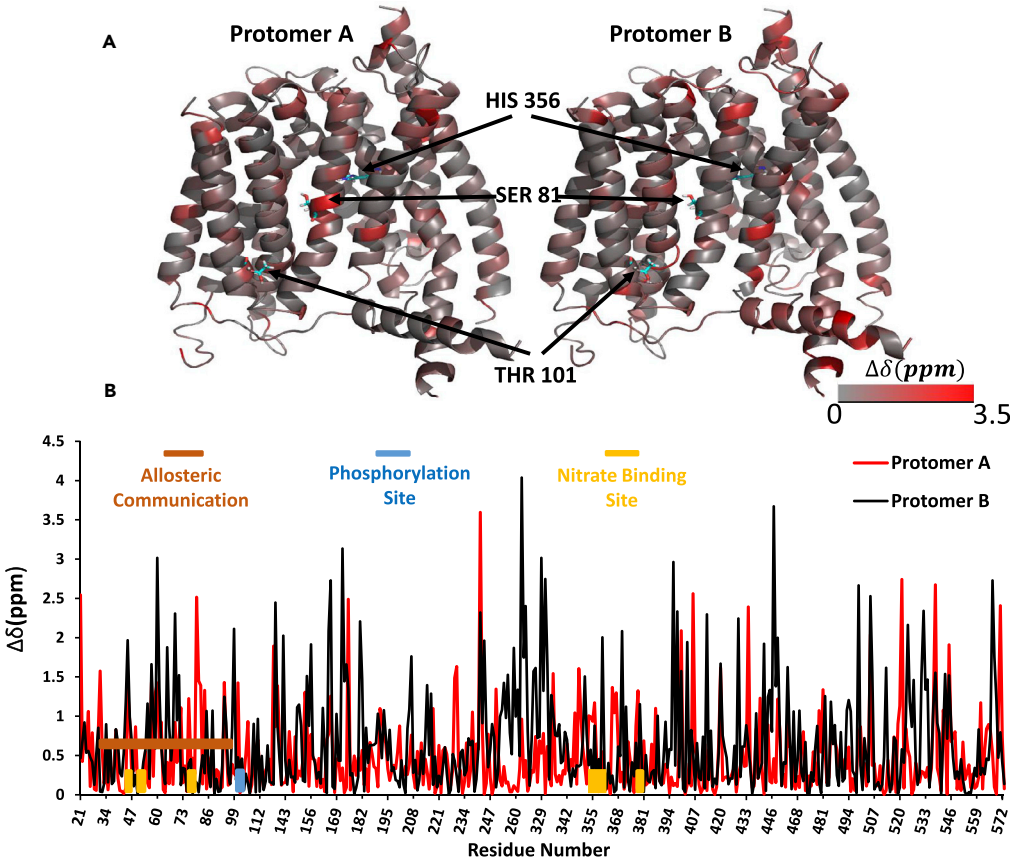

Figure 3. Differences between $^{13}C\alpha$ Backbone Chemical Shift ($\Delta\delta$ ppm) of Both the Protomers A and B

(A) Differences are projected onto the NRT1.1 secondary structure, and (B) several regions are identified in which larger differences are observed.

regions are shown to exhibit larger chemical shift differences associated with nitrate-triggered allostery: region of allosteric communication [30–94], nitrate-binding pocket, and phosphorylation sites Thr 101 (Figure 3B).

To examine whether nitrate-triggered structural asymmetries between the protomers have any functional consequences, CSM algorithm has been implemented for calculating the nitrate-binding affinities ($-\log_{10}k_D/k_i$) with the inputs of NRT1.1 nitrate-bounded structures in CSM-lig web server (Pires and Ascher, 2016). CSM is a class of graph-based signatures in which atoms are seen as nodes and binding interactions as edges. It extracts distance patterns between the interacting components, defining the complementarity between the proteins and binding molecule based on their shapes and chemistry. This examination has shown that the two protomers hold differential binding affinities. Protomer A has the nitrate-binding affinities of −78.7 kcal/mol, whereas protomer B has the affinity of −16.5 kcal/mol.

Intraprotomer Allosteric Communications

To prime Thr 101 site for phosphorylation with the initiation of nitrate binding, a certain amount of inflexibilities of both the protomers are essential. Rigidity analysis of protein structure based on the fundamental molecular theorem (Katoh and Tanigawa, 2011) is useful for determining and characterizing the mode and the nature of allostery. A network formed by considering all the types of chemical bonds (covalent, electrostatic, hydrophobic, and H-bonds) from a given protein conformation is used in forming rigid clusters. Rigidity-theory-based allostery analysis (Jacobs et al., 2001; Chubynsky and Thorpe, 2007) was carried out in the KINARI (http://kinari.cs.umass.edu), which uses pebble game algorithm (Jacobs and Hendrickson, 1997) with the inputs of apo- and nitrate-bound crystal structures. The KINARI outputs showed that the total degree of freedom reduces significantly with reduction in the number of rigid bodies of atoms

Parameters	Protomer A		Protomer B	
	NO_3^- Unbounded	NO_3^- Bounded	NO_3^- Unbounded	NO_3^- Bounded
No. of H-bonds	341	347	346	349
No. of hinges	1591	1362	1420	1434
No. of bars	278	230	224	248
No. of bodies	1532	1323	1379	1395
No. of Degrees of Freedom	953	892	944	946

Table 1. Summary of Different Parameters of Rigidity Analysis

(clusters) in protomer A after nitrate binding as compared with protomer B (Table 1). This indicates that nitrate triggered more changes in chemical interactions in protomer A, leading to redistribution of rigid clusters of atoms, making it relatively more rigid than protomer B.

In particular, further analysis of the rigid clusters shows that there exists a *largest rigid cluster* (LRC) [30–94] in the nitrate-bound protomer A, which bridges the residues of the nitrate-binding pocket to the residues of the phosphorylation site (Figure 4, Table 2). Of relevance to allostery, this resulting rigid cluster measures the extent of allosteric communication. Specifically, a fraction of atoms that belongs to the LRC gives

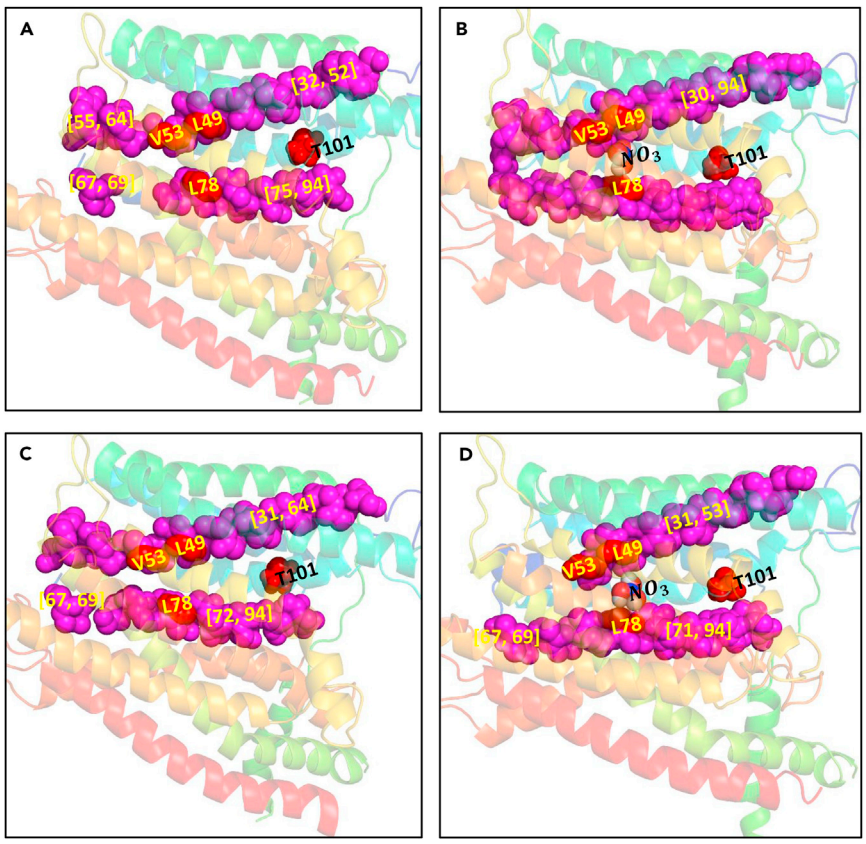

Figure 4. Largest Rigid Cluster [30–94]

In protomer A, the LRC (magenta balls) connects the residues of the nitrate-binding pocket to the phosphorylation site. L49, V53, and L78 are the binding pocket residues, T101 is the phosphorylation site, and the residues within brackets are the clusters formed before and after nitrate binding in protomers A and B of NRT1.1. (A) Nitrate unbound protomer A. (B) Nitrate bound protomer A. (C) Nitrate unbound protomer B. (D) Nitrate bound protomer B.

Parameters	Nitrate-Unbound Protomer A [30, 94]	Nitrate-Bound Protomer A [30, 94]
Rigid clusters	[32, 52], [55, 64], [67, 69], [75, 94]	[30, 94]
No. of H-bonds	46	49
H-bonds broken in [30, 94] after NO_3^- binding	Ala32-Met36, Ser33-Ile37, Met36-Cys39, Glu44-Thr47, Arg45-Leu49, Thr48-Gly52, Thr57-Thr60, Tyr58-Thr62, Leu59-Leu65, Ala70-Thr73, Asn72-Thr75, Ile91-Thr94	
Newly added H-bonds in [30, 94] after NO_3^- binding	Gly30-Ser33, Ile37-Cys39, Val43-Thr47, Glu44-Arg45, Glu44-Thr48, Asn54-Val56, Thr69-Thr73, Ala71-Val74, Ala71-Thr75, Phe77-Ser81, Leu78-Phe82, Ser81-Cys85, Leu86-Phe90, Phe90-Thr94, Phe90-Thr94	
No. of H-bonds conserved in [30, 94] before and after NO_3^- binding	34	

Table 2. Summary of the Rigidity-Based Allosteric Analyses

a quantitative measure of the degree of structural coupling and rigidity-based allostery within the protein: $X_{LRC} = N_{LRC}/N$ (N is the total number of atoms and N_{LRC} is the number of atoms in the LRC). The difference $\Delta X_{LRC} = X_{LRC}^{unbound} - X_{LRC}^{bound} = 0.05 - 0.23 = -0.18 < 0$ (negative value) indicates that nitrate binding triggers rigidity-based allostery in the nitrate-bounded NRT1.1 (Rader and Brown, 2011). Such a rigid cluster has not been predicted in protomer B, indicating weak or absent allosteric communication between the binding and Thr 101 sites.

To determine the fraction of nitrate-binding site and Thr101 site residues in the LRC in either of the apo and nitrate-bound protomers, we calculated

$$Z_{LRC}^{A,\ NO_3-unbounded} = 0.24,\quad Z_{LRC}^{A,\ NO_3-bounded} = 0.12,$$
$$Z_{LRC\_T101}^{A,\ NO_3-unbounded} = 0.52,\quad Z_{LRC\_T101}^{A,\ NO_3-bounded} = 0.23$$

The positive values of these expressions along with ΔX_{LRC} indicate that the nitrate binding is the main source of changes in the rigidity of protomer A (Rader and Brown, 2011). In contrast, there does not exist such an LRC for allostery in protomer B (Figure 4). This analysis, therefore, suggests that nitrate-induced conformational changes establish a rigidity-based allosteric communication between the nitrate-binding site and the Thr 101 site, which is responsible for priming Thr 101 for phosphorylation.

A study of the formation and dilution of H-bonds within the rigid cluster shows that nitrate binding has triggered the addition and re-distribution of H-bonds (Figures 5, S5, and Table 2) through conformational changes, resulting in strong allosteric communication between the distant sites in protomer A. This result is further supported by the crystallographic B-factors distribution within the clusters that shows rapid internal fluctuations upon the initiation of nitrate binding (Figure 6). The rigidity-based allosteric cluster remains

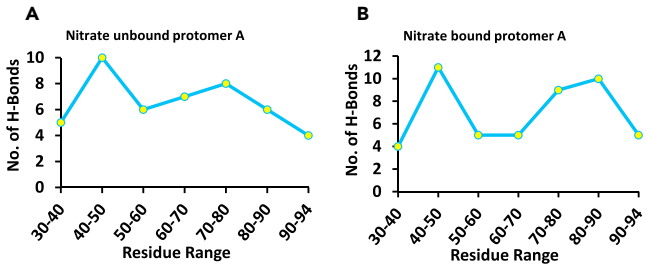

Figure 5. Distribution of H-bonds before and after Nitrate Binding

Nitrate-binding has triggered the re-distribution of H-bonds through conformational changes, resulting in strong allosteric communication between the nitrate-binding and phosphorylation site T101 through the formation of a large rigid cluster. (A and B) (A) before Nitrate Binding, and (B) after Nitrate Binding.

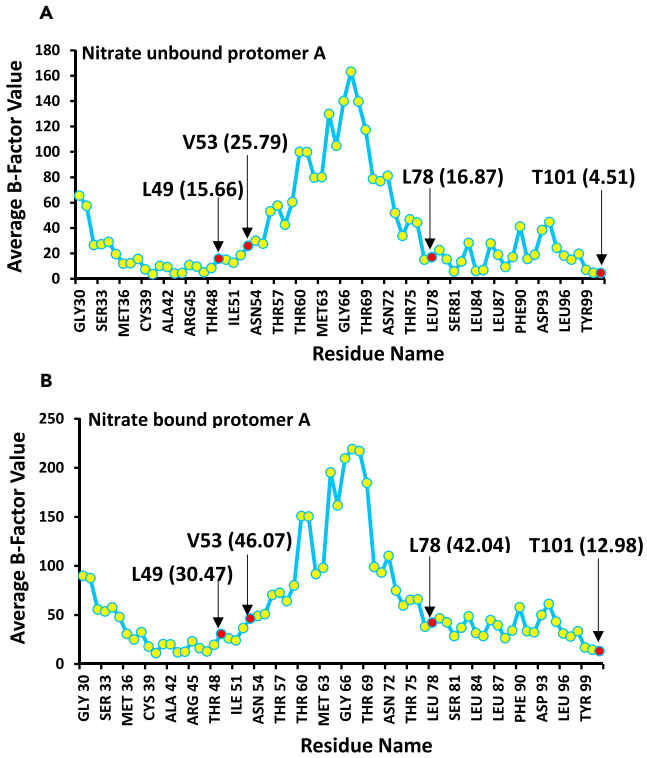

Figure 6. Crystallographic B-factor Distribution within the Rigid Cluster

It is responsible for allosteric communication in protomer A, indicating rapid internal fluctuations upon the initiation of nitrate binding. (A and B) (A) before Nitrate Binding, and (B) after Nitrate binding.

rigid as the entropic cost (loss of energy from 276.2 to 218.63 kcal/mol) associated with the nitrate binding is compensated for by an increase in B-factors.

In Silico Mutational Analysis

To identify key residues in the allosteric communication pathway [30–94], all possible *in silico* mutational analyses have been carried out in protomer A of the NRT1.1 crystallographic structure (Table S4). This method is calibrated with the experimental results of Ho et al. (2009) in which single amino acid mutants Thr101Asp (T101D) and Thr101Ala (T101A) mimicked phosphorylated and de-phosphorylated states of

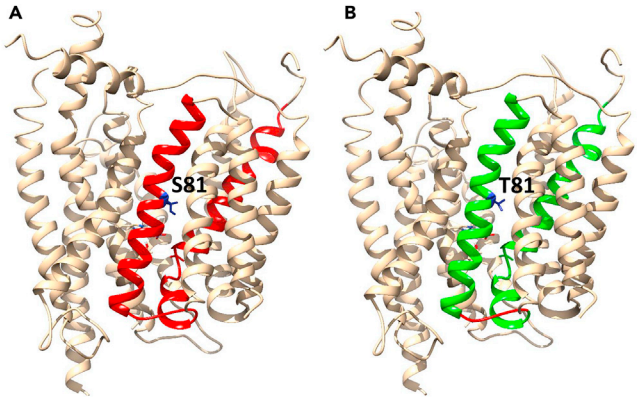

Figure 7. Mutational Analysis of Ser81Thr

Mutation of Ser 81 to Thr splits the largest rigid cluster (LRC) (A: red) into two different pieces (B: green), indicating the key role of Ser 81 in maintaining the allosteric communication pathways within the LRC.

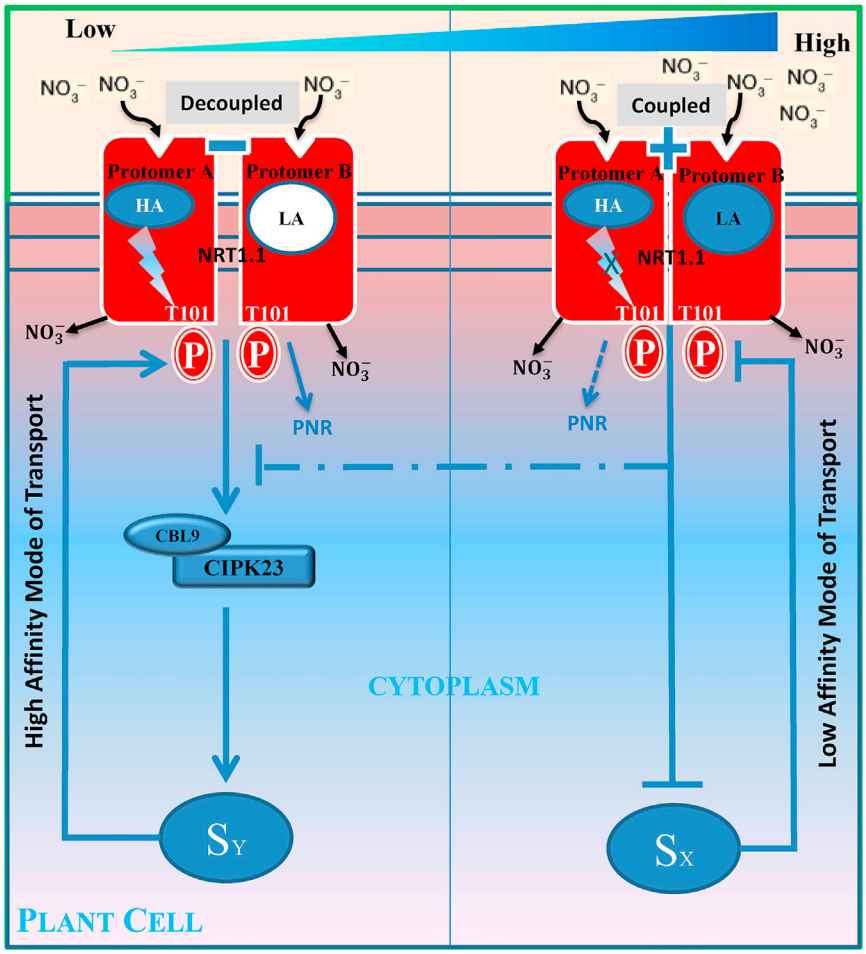

Figure 8. A Model of Phosphorylation Switch

Protomer A contains a high-affinity nitrate-binding site, whereas protomer B contains a relatively low-affinity binding site. Binding of nitrate ion triggers an allosteric communication between the binding site and the T101 site in protomer A that primes the T101 site for phosphorylation and is responsible for activating the immediate downstream component of the nitrate signaling CBL9.CIPK23 complex at low nitrate concentration. In contrast, such an allosteric communication pathway is absent in protomer B. At low nitrate concentrations, nitrate ion binds only at the high-affinity site of protomer A and activates the CBL9.CIPK23 complex. At high nitrate concentrations, nitrate binds to both the sites of protomer A and protomer B and then continuously inhibits the activity of the CBL9.CIPK23 complex along the increasing gradient of nitrate.

NRT1.1, respectively. In parallel to this experimental result, we showed that T101A breaks the rigid cluster that is responsible for allosteric communication into two distinct clusters, whereas the T101D retains the intact allosteric rigid cluster. It, therefore, suggests that priming of the T101 site in protomer A for the phosphorylation is allosterically triggered by the high-affinity nitrate binding, whereas in protomer B such allosteric communication is weak or absent. It has further been noted that most of the new H-bonds in protomer A are added at the sites 80–90 (Figure 5), from which residues are chosen for mutational analysis. The analysis showed that Ser 81 is one of the potential key residues for maintaining the allosteric communication pathway. With the mutations of Ser81Thr, Ser81Val, and Ser81Asp, the allosteric rigid cluster splits into two distinct clusters owing to the loss of H-bonds between Ser 81 and Phe 77, and Ser 81 and Cys 85, which were added through nitrate binding (Figure 7).

DISCUSSION

NRT1.1 acts like a toggle switch through the phosphorylation of Thr101, a functional switch for biphasic regulation of nitrate signaling and uptake. Phosphorylation of NRT1.1 at T101 leads to switching from

low-affinity to high-affinity transport modes (Liu and Tsay, 2003). Besides, it is also responsible for down-regulating the PNR at low soil nitrate concentrations. For this phosphorylation, activation of calcineurin B-like protein CBL9-interacting kinase CIPK23 is essential at the downstream nitrate singling pathways (Leran et al., 2015). Nitrate binding to NRT1.1 is responsible for creating calcium waves through the action of an unknown phospholipase C, and blocking these waves severely affects several nitrate-induced responses (Riveras et al., 2015; Armijo and Gutiérrez, 2017). Activities of the CBL9.CIPK23 complex toward NRT1.1 depend on these calcium waves (Ho et al., 2009; Leran et al., 2015). Our structural analysis further indicates that the intrinsic asymmetries between the two protomers of NRT1.1 may also differentially affect the magnitude of this calcium wave via the dimerization switch and thereby the activities of the CIPK23 complex, as these asymmetries are differentially enhanced by the high- and low-affinity modes of nitrate binding controlling dimer disassembly and assembly, respectively.

Asymmetries between the two protomers of NRT1.1 are enhanced by nitrate binding and caused for holding dual-affinity binding of nitrate. Protomer A contains a high-affinity nitrate-binding site, whereas protomer B contains a relatively low-affinity binding site. Binding of nitrate ion triggers an allosteric communication between the binding site and the T101 site in protomer A that primes the Thr 101 site for phosphorylation and is responsible for activating the immediate downstream component of nitrate signaling CBL9.CIPK23 complex at low nitrate concentration. In contrast, such an allosteric communication pathway is absent in protomer B. This intramolecular allostery possibly generates two distinct signals: one that activates calcineurin B-like protein CBL9-interacting kinase CIPK23 complex by creating specific cytoplasmic calcium waves at low nitrate concentration (S_Y) and the other that negatively regulates the activity of the kinase complex at high nitrate concentration (S_X). At low nitrate concentration, nitrate ion binds only at the high-affinity site of protomer A and activates the CBL9.CIPK23 complex. At a high nitrate concentration, nitrate binds to both the sites of protomer A and protomer B and then continuously inhibits the activity of the CBL9.CIPK23 complex along the increasing gradient of nitrate (Figure 8). It therefore may generate two distinct regulatory effects of nitrate binding: one that positively regulates the NRT1.1 phosphorylated state and the other that negatively controls this state.

METHODS

All methods can be found in the accompanying Transparent Methods supplemental file.

SUPPLEMENTAL INFORMATION

Supplemental Information includes Transparent Methods, six figures, and four tables and can be found with this article online at https://doi.org/10.1016/j.isci.2018.03.007.

ACKNOWLEDGMENTS

Our thanks to all our colleagues and the members of the School of Mathematics, Statistics and Computational Sciences, Central University of Rajasthan (CURaj) for their support in completing this work. We highly appreciate Dr. Yi-Fang Tsay, Institute of Molecular Biology, Academia Sinica, Taiwan, for her critical comments on the previous version of this manuscript. This research was partially supported by DST-SERB grant (file no. EMR/2015/001671) and by the Central University of Rajasthan; M.R. and S.B. received their PhD fellowships from the CURaj.

AUTHOR CONTRIBUTIONS

M.R., S.B., A.C. designed the study and conducted computational experiment and analytical analysis. A.C., M.R., G.-Q.S., A.B.M. and B.-L.L. have reviewed and written the article.

DECLARATION OF INTERESTS

The authors declare no conflict of interest.

Received: December 4, 2017
Revised: February 12, 2018
Accepted: February 22, 2018
Published: April 27, 2018

REFERENCES

Armijo, G., and Gutiérrez, R.A. (2017). Emerging players in the nitrate signaling pathway. Mol. Plant *10*, 1019–1022.

Bouguyon, E., Brun, F., Meynard, D., Kubes, M., Pervent, M., Leran, S., Lacombe, B., Krouk, G., Guiderdoni, E., Zažímalová, E., et al. (2015). Multiple mechanisms of nitrate sensing by Arabidopsis nitrate transceptor NRT1.1. Nat. Plants *1*, 1–8.

Chubynsky, M.V., and Thorpe, M.F. (2007). Algorithms for three-dimensional rigidity analysis and a first-order percolation transition. Phys. Rev. E. Stat. Nonlin. Soft. Matter Phys. *76*, 041135.

Crawford, N.M. (1995). Nitrate: nutrient and signal for plant growth. Plant Cell *7*, 859–868.

Crawford, N.M., and Glass, A.M. (1998). Molecular and physiological aspects of nitrate uptake in plants. Trends Plant Sci. *3*, 1360–1385.

Giehl, R.F.H., and von Wirén, N. (2015). Functions of a nitrate transceptor. Nat. Plants *1*, 15021.

Good, A.G., Shrawat, A.K., and Muench, D.G. (2004). Can less yield more? Is reducing nutrient input into the environment compatible with maintaining crop production? Trends Plant Sci. *9*, 597–605.

Gutiérrez, R.A. (2012). Systems biology for enhanced plant nitrogen nutrition. Science *336*, 1673–1675.

Han, B., Liu, Y., Ginzinger, S.W., and Wishart, D.S. (2011). SHIFTX2: significantly improved protein chemical shift prediction. J. Biomol. NMR *50*, 43–57.

Ho, C.H., Lin, S.H., Hu, H.C., and Tsay, Y.F. (2009). CHL1 functions as a nitrate sensor in plants. Cell *138*, 1184–1194.

Jacobs, D.J., and Hendrickson, B. (1997). An algorithm for two-dimensional rigidity percolation: the pebble game. J. Comput. Phys. *137*, 346–365.

Jacobs, D.J., Rader, A.J., Kuhn, L.A., and Thorpe, M.F. (2001). Protein flexibility predictions using graph theory. Proteins *44*, 150–165.

Katoh, N., and Tanigawa, S.I. (2011). A proof of the molecular conjecture. Discrete Comput. Geom. *45*, 647–700.

Krouk, G. (2017). Calcium bridges the nitrate gap. Nat. Plants *3*, 17095–17096.

Krouk, G., Crawford, N.M., Coruzzi, G.M., and Tsay, Y.F. (2010). Nitrate signaling: adaptation to fluctuating environments. Curr. Opin. Plant Biol. *13*, 266–273.

Krouk, G., Tillard, P., and Gojon, A. (2006). Regulation of the high-affinity nitrate uptake system by NRT1.1-mediated NO3- demand signaling in Arabidopsis. Plant Physiol. *142*, 1075–1086.

Leran, S., Edel, K., Pervent, M., Hashimoto, K., Corratgé-Faillie, C., Offenborn, J., Tillard, P., Gojon, A., Kudla, J., and Lacombe, B. (2015). Nitrate sensing and uptake in Arabidopsis are enhanced by ABI2, a phosphatase inactivated by the stress hormone abscisic acid. Sci. Signal. *8*, ra43.

Liu, K.H., Huang, C.Y., and Tsay, Y.F. (1999). CHL1 is a dual-affinity nitrate transporter of Arabidopsis involved in multiple phases of nitrate uptake. Plant Cell *11*, 865–874.

Liu, K.H., and Tsay, Y.F. (2003). Switching between the two action modes of the dual-affinity nitrate transporter CHL1 by phosphorylation. EMBO J. *22*, 1005–1013.

Medici, A., and Krouk, G. (2014). The primary nitrate response: a multifaceted signalling pathway. J. Exp. Bot. *65*, 5567–5576.

Nacry, P., Bouguyon, E., and Gojon, A. (2013). Nitrogen acquisition by roots: physiological and developmental mechanisms ensuring plant adaptation to a fluctuating resource. Plant Soil *370*, 1–29.

Parker, J.L., and Newstead, S. (2014). Molecular basis of nitrate uptake by the plant nitrate transporter NRT1.1. Nature *507*, 68–72.

Pires, D.E., and Ascher, D.B. (2016). CSM-lig: a web server for assessing and comparing protein-small molecule affinities. Nucleic Acids Res. *44*, 557–561.

Rader, A.J., and Brown, S.M. (2011). Correlating allostery with rigidity. Mol. Biosyst. *7*, 464–471.

Riveras, E., Alvarez, J.M., Vidal, E.A., Oses, C., Vega, A., and Gutierrez, R.A. (2015). The calcium ion is a second messenger in the nitrate signalling pathway of Arabidopsis. Plant Physiol. *169*, 1397–1404.

Sun, J., Bankston, J.R., Payandeh, J., Hinds, T.R., Zagotta, W.N., and Zheng, N. (2014). Crystal structure of the plant dual-affinity nitrate transporter NRT1.1. Nature *507*, 73–77.

Tsay, Y.F. (2014). How to switch affinity. Nature *507*, 44–45.

von Wirén, N., Gazzarrini, S., Gojon, A., and Frommer, W.B. (2000). The molecular physiology of ammonium uptake and retrieval. Curr. Opin. Plant Biol. *3*, 254–261.

Wang, R., Tischner, R., Gutierrez, R.A., Hoffman, M., Xing, X., Chen, M., Coruzzi, G., and Crawford, N.M. (2004). Genomic analysis of the nitrate response using a nitrate reductase-null mutant of Arabidopsis. Plant Physiol. *136*, 2512–2522.

Wang, M.Y., Siddiqi, M.Y., Ruth, T.J., and Glass, A.D.M. (1993). Ammonium uptake by rice roots. (I. Fluxes and subcellular distribution of $^{13}NH_4^+$). Plant Physiol. *103*, 1249–1258.

Williams, L.E., and Miller, A.J. (2001). Transporters responsible for the uptake and partitioning of nitrogenous solutes. Annu. Rev. Plant Physiol. Plant Mol. Biol. *52*, 659–688.

ISCI, Volume *2*

Supplemental Information

Adaptive Regulation of Nitrate Transceptor NRT1.1 in Fluctuating Soil Nitrate Conditions

Mubasher Rashid, Soumen Bera, Alexander B. Medvinsky, Gui-Quan Sun, Bai-Lian Li, and Amit Chakraborty

Supplemental figures and legends

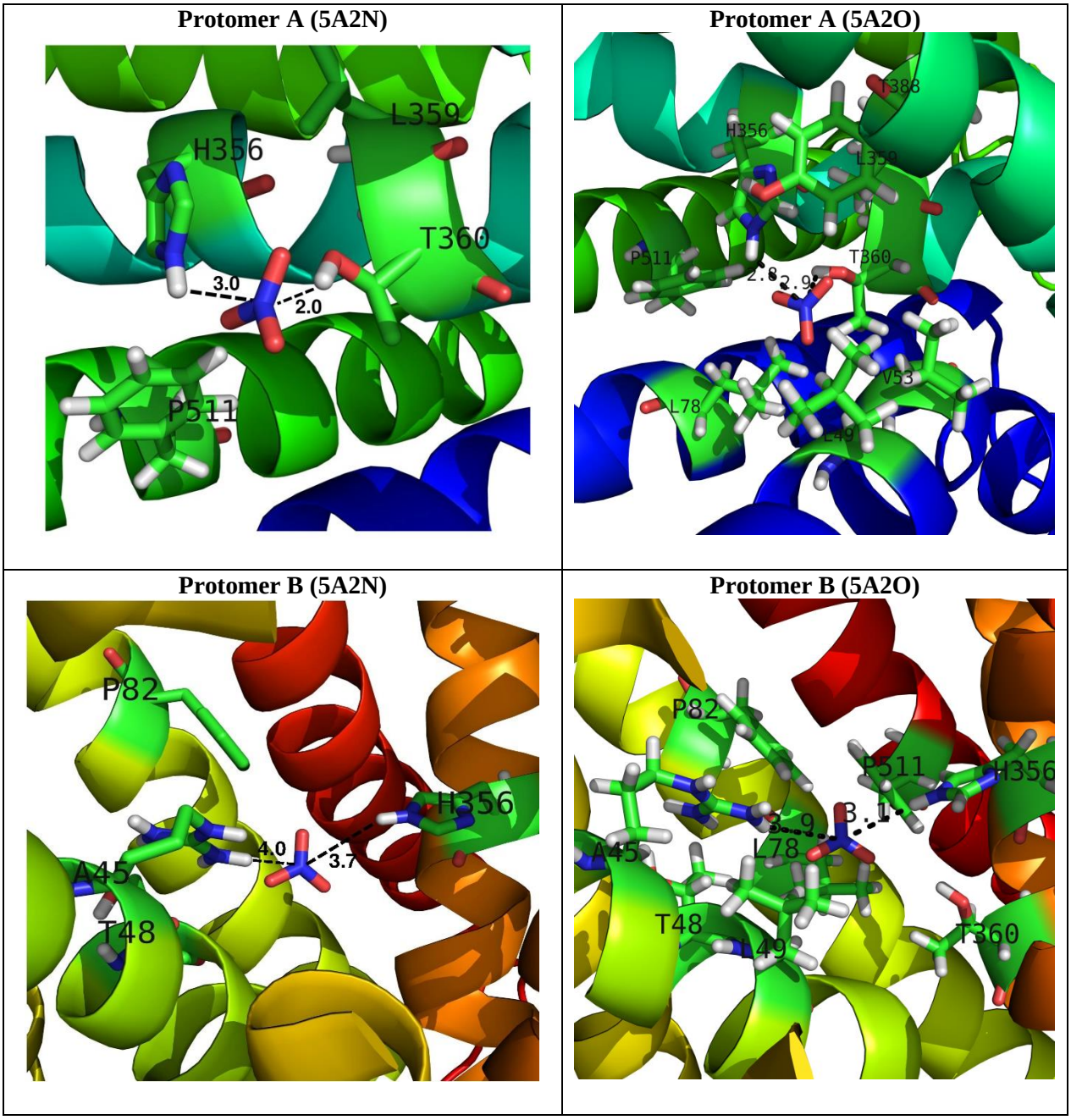

Figure S1. Close up of neighbourhood residue compositions around nitrate within the distance of 4.0 Å, related to Figure 1 and interprotomer asymmetries. It shows differential neighbourhood compositions between the protomers.

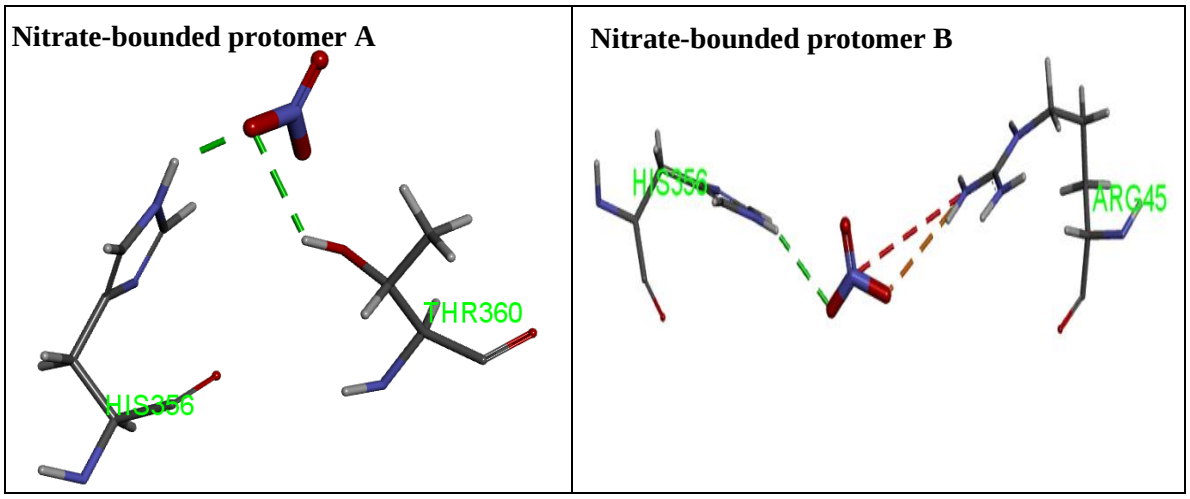

Figure S2. H-bond interactions between nitrate and amino acid residues in protomers A and B, related to Figure 1 and interprotomer asymmetries and differential nitrate-binding affinities. Nitrate interacts with HIS 356 and THR 360 in the nitrate bounded protomer A, whereas it interacts with HIS 356 and ARG 45 in the protomer B.

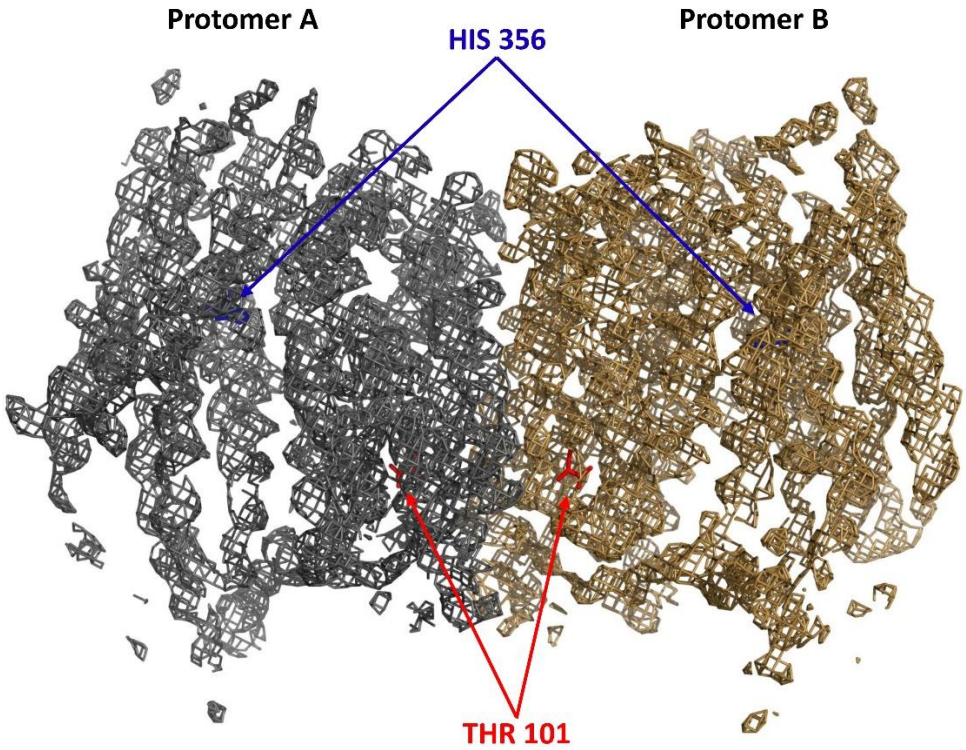

Figure S3. View of $2F_o$ - F_c density map contoured at 2.0 δ, related to Figure 2 and interprotomer asymmetries. It shows the local asymmetry at nitrate binding site residue (blue arrow) and phosphorylation site residue (red arrow).

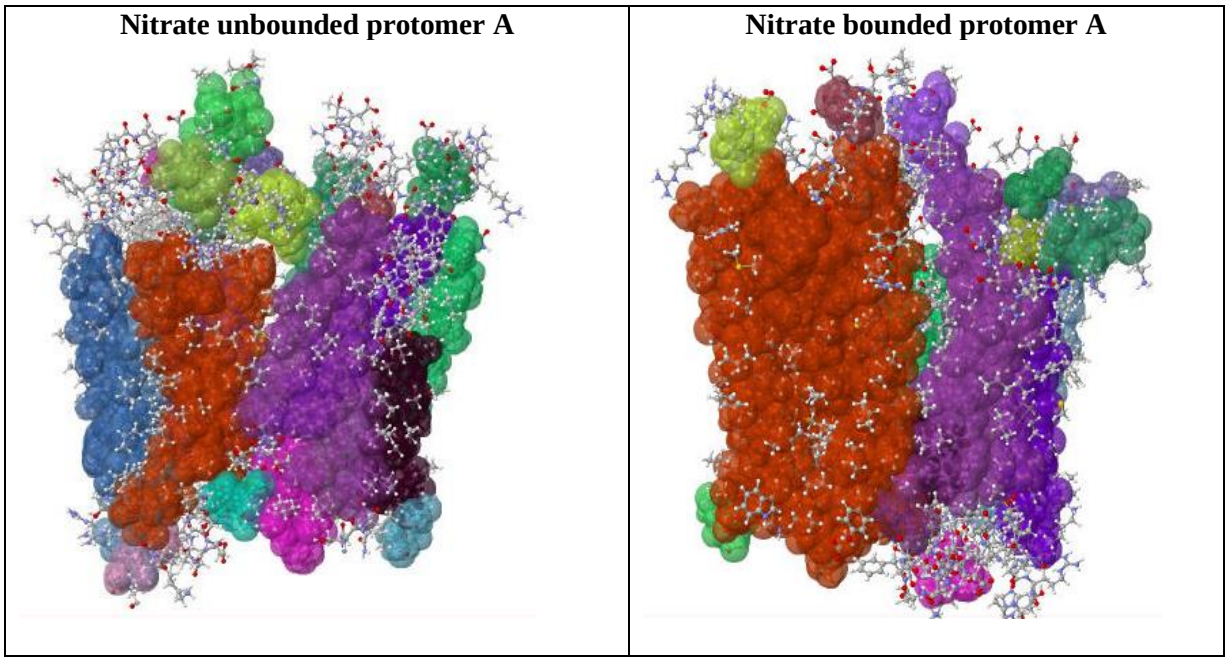

Figure S4. Comparison of rigid cluster distribution in protomer A of NRT1.1, related to Figure 4 and intraprotomer allosteric communications. Red colour denotes largest rigid cluster. This rigid cluster becomes even more large in nitrate bounded protomer A containing residues [30, 94] spanning between nitrate binding pocket and Thr 101 site.

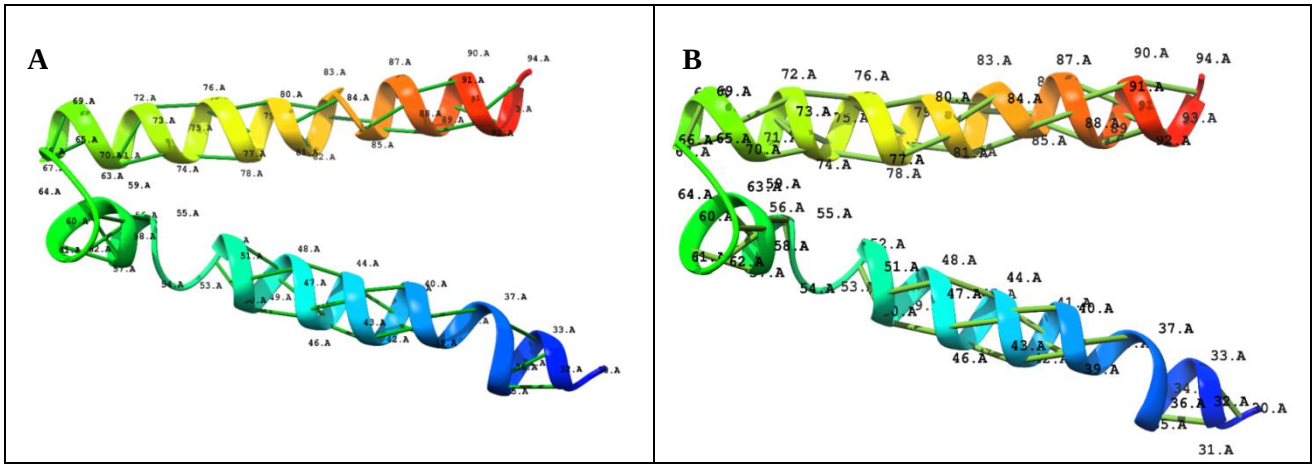

Figure S5. Visual illustration of distribution of H-bonds, related to Figure 5 and intraprotomer allosteric communications. Nitrate unbounded protomer A (A), and nitrate bounded protomer A (B) in the residue range [30, 94]. After nitrate binding (B) there is redistribution of hydrogen bounds and also few more hydrogen bonds are added in this cluster.

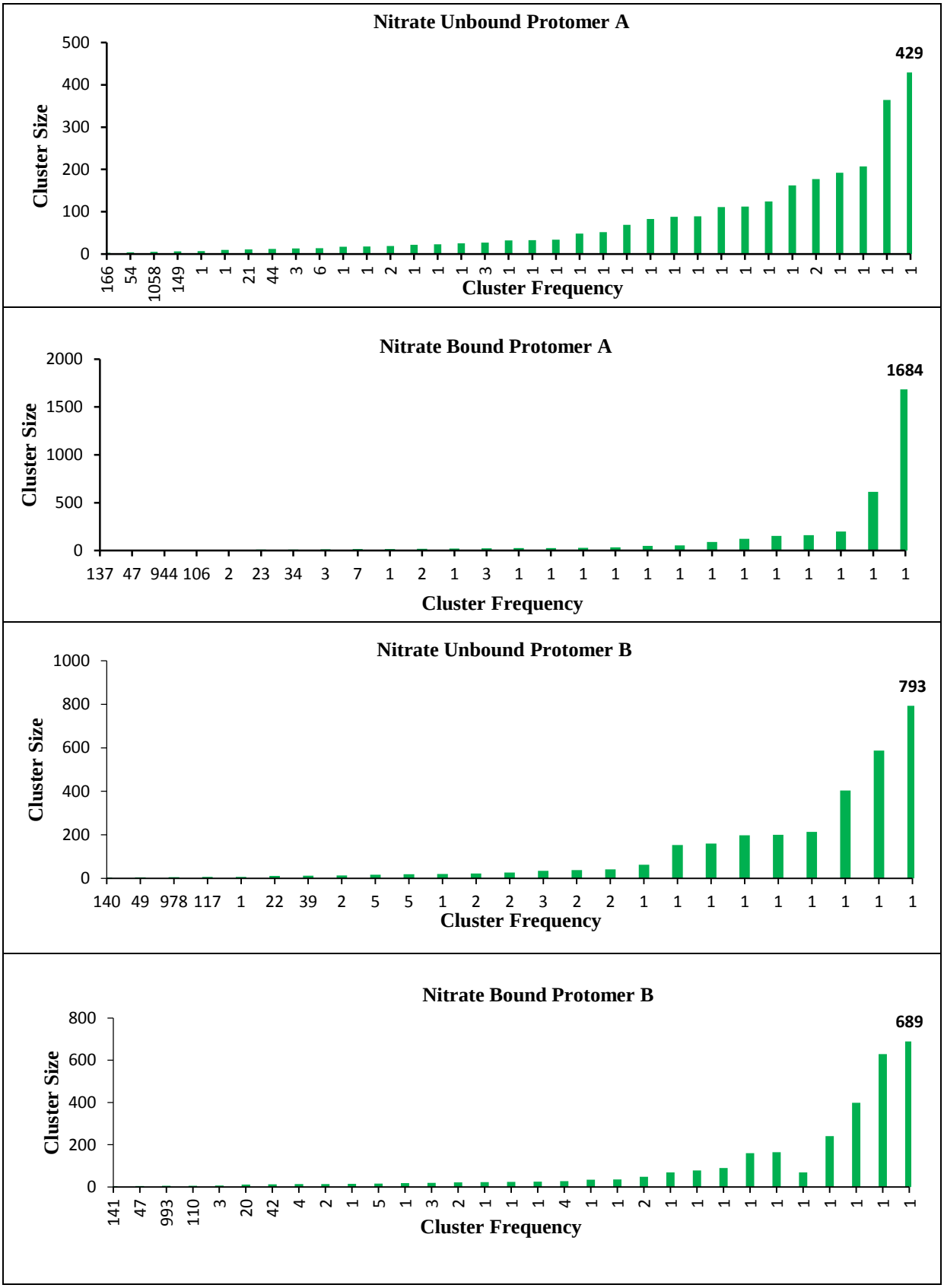

Figure S6. Bar graphs display frequency and size of rigid clusters in apo and nitrate bounded protomers of NRT1.1., related to Figure 4 and intraprotomer allosteric communications. In nitrate bound protomer A, there is a large cluster consisting of 1684 atoms which spans between nitrate binding site and Thr101 site. However no such cluster has been found in any of the other protomers.

Supplemental tables

Table S1: Compositional differences between the nitrate-bounded and unbounded NRT1.1, related to Figure 2 and interprotomer asymmetries.

	NRT1.1 apo-protein (5A2N)		NRT1.1 nitrate-bounded protein (5A2O)	
	Nitrate neighbourhood (4.0 Å)	**Thr101 neighbourhood (4.0 Å)**	**Nitrate neighbourhood (4.0 Å)**	**Thr101 neighbourhood (4.0 Å)**
Protomer A	Leu 49, His 356, Leu 359, Thr 360, Tyr 388, Phe 511	Gly 88, Ile 91, Ala 92, Gly 97, Arg 98, Tyr 99, Leu 100, Ile 102, Ala 103, Ile 104, Phe 105, Gly 162, Ser 166	Leu 49, Val 53, Leu 78, His 356, Leu 359, Thr 360, Tyr 388, Phe 511	Gly 88, Ile 91, Ala 92, Gly 97, Arg 98, Tyr 99, Leu 100, Ile 102, Ala 103, Ile 104, Phe 105, Ala 106, Gly 162, Val 163, Ser 166
Protomer B	Arg 45, Thr 48, Leu 49, Phe 82, His 356	Gly 88, Ile 91, Ala 92, Gly 97, Arg 98, Tyr 99, Leu 100, Ile 102, Ala 103, Ile 104, Phe 105, Ala 106, Gly 162, Val 163, Ala 165, Ser 166	Arg 45, Thr 48, Leu 49, Leu 78, Phe 82, His 356, Thr 360, Phe 511	Gly 88, Ile 91, Ala 92, Gly 97, Arg 98, Tyr 99, Leu 100, Ile 102, Ala 103, Ile 104, Phe 105, Ala 106, Gly 162, Val 163, Ala 165, Ser 166

Table S2: Summary of changes in allowed regions of dihedral angles, related to Figure 1.

Nitrate unbounded protomer A	Nitrate bounded protomer A	Nitrate unbounded protomer B	Nitrate bounded protomer B
HIS 356 (-58.62, -46.40)	**HIS356 (-76.65, -30.76)**	**HIS 356 (-77.36, -27.82)**	**HIS 356 (-71.49, -35.86)**
THR 360 (-80.38, -31.38)	**THR 360 (-77.17, -40.27)**	**ARG 45 (-55.82, -40.33)**	**ARG 45 (-63.89, -67.96)**
THR 101 (-59.49, -47.27)	**THR 101 (-62.12, -31.32)**	**THR 101 (-63.87, -36.67)**	**THR 101 (-68.20, -41.31)**

Table S3: Interface statistics, related to Figure 3.

	NRT1.1 Apo-protein (5A2N)			NRT1.1 nitrate-bounded protein (5A2O)		
	Interface area ($Å^2$)	**No. of interface residues**	**No. of hydrogen bonds**	**Interface area ($Å^2$)**	**No. of interface residues**	**No. of hydrogen bonds**
Protomer A	**1093**	**21**	**04** **Thr111 --Val229** **Thr111--Ser233** **Thr111--Ser233** **Val229--Thr11**	**1087**	**20**	**01** **Ser233--Thr111**
Protomer B	**1099**	**23**		**1078**	**21**	

Table S4: Summary of mutational analysis, related to Figure 7 and *in silico* mutational analysis					
Mutation [80-90]	**Cluster Break(Y/N)**	**No. of clusters formed**	**No. of h-bonds in the allosteric rigid cluster [30-94]**	**ΔΔG (Mutant -WT) Kcal/mol**	**Stability**
Thr101Asp **(T101D)**	N	1	53	2.45	Highly Destabilizing
Thr101Ala **(T101A)**	Y	2	53	0.45	Neutral
Thr80Ala	N	1	55	-0.83	Slightly Stabilizing
Thr80Asp	N	1	53	-0.18	Neutral
Thr80His	N	1	55	-0.97	Stabilizing
Thr80Leu	Y	2	54	-2.38	Highly Stabilizing
Thr80Pro	N	1	52	4.26	Highly Destabilizing
Thr80Ser	Y	2	55	-0.38	Neutral
Thr80Val	N	1	54	-0.63	Slightly Stabilizing
Ser81Ala	N	1	55	-0.39	Neutral
Ser81Asp	Y	2	53	3.33	Highly Destabilizing
Ser81His	N	1	53	3.61	Highly Destabilizing
Ser81Leu	N	1	55	1.27	Destabilizing
Ser81Pro	N	1	53	4.65	Highly Destabilizing
Ser81Thr	Y	2	56	0.89	Slightly Destabilizing
Ser81Val	Y	2	53	0.59	Slightly Destabilizing
Leu84Ala	N	1	55	1.91	Highly Destabilizing
Leu84Asp	Y	2	57	3.26	Highly Destabilizing
Leu84His	N	1	54	1.01	Destabilizing
Leu84Pro	Y	2	54	6.11	Highly Destabilizing
Leu84Ser	N	1	54	2.74	Highly Destabilizing
Leu84Thr	Y	2	55	1.64	Destabilizing
Leu84Val	N	1	55	0.40	Neutral

Transparent Methods

Visual analysis of neighbourhoods

Comparative visual analyses of apo- and nitrate bounded crystallographic structures presents the differences in 4.0 Å neighbourhoods of nitrate and Thr101 phosphorylation site (Table S1). Nitrate and Thr101 neighbourhoods have been determined by using PyMOL v1.7.2.1 (DeLano, 2006). To determine nitrate neighbourhoods in nitrate-unbounded protomers of apo-protein, nitrate has been separated from the two protomers of nitrate bounded crystallographic structure in PyMOL and then superimposed in the respective unbounded protomers of apo-protein.

Interactions of nitrate in the binding sites of two protomers of NRT1.1 have been determined in UCSF Chimera (version 1.11.2) (Pettersen et al., 2004). It was further verified in BIOVIA Discovery Studio v16.1.0. While in protomer A, nitrate showed interactions with the residues His 356 and Thr 360, in protomer B Thr 360 was replaced by Arg 45 (Figure S1, S2). These residues are also in close proximity to nitrate among other neighbouring residues.

Visual analysis shows that in protomer A of NRT1.1, residues Thr 360 and His 356 are in close proximity to nitrate, while as in protomer B residues Arg 45 and His 356 are closer to nitrate. Ramachandran plot (Ramachandran et al., 1963) has been used to illustrate the changes in energetically allowed regions of the backbone dihedral angles. In particular comparative analysis using Visual Molecular Dynamics (version 1.9.3beta4) (Humphrey et al., 1996) has identified significant changes in allowed regions of Phi and Psi angles in the residues Thr360, His 356, Arg45, and the phosphorylation site Thr101 before and after nitrate binding (Table S2).

We have used PDBePISA (www.ebi.ac.uk/pdbe/pisa), a web-based interactive tool, for analysing the interfaces between the protomers of NRT1.1 nitrate-unbounded and bounded crystals. The interface of apo-structure with the interfacing area A.1093 Å² and B.1099 Å², besides the non-bonded contacts, the only bonded contacts present are four hydrogen bonds: A.Thr111 --B.Val229, A.Thr111--B.Ser233, A.Thr111--B.Ser233, A.Val229--B.Thr11. After nitrate binding, all the four interactions are completely lost with reduced interfacing surface area, building a single new H-bond between A.Ser233-B.Thr111 (Table S3).

Electron Density Map

To examine the intrinsic local structural asymmetry between the two protomers in the asymmetric units, we used CCP4 maps (Jones et al., 1991; Winn et al., 2011) to produce $2F_o$-F_c electron density map contoured at 2.0 σ (Figure S3). A closed view at the binding site (blue) and phosphorylation site (red) of the two protomers shows different conformations of the residues involving these sites. While His 356 in protomer A and Thr 101 in protomer B surfaced out, His 356 in protomer B and Thr 101 in protomer A are comparatively buried. We have also observed that this asymmetry is sustained and further differentially enhanced after nitrate binding.

Chemical shifts

To predict differences in chemical shifts between the nitrate bounded and unbounded protomers, SHIFTX2 (http://www.shiftx2.ca) has been used with inputs of apo-and nitrate bounded crystal structures of *Arabidopsis thaliana* NRT1.1. It correlates intrinsic interprotomer asymmetry with the nitrate-bounded states, with the differences between backbone chemical shifts, $^{13}C\alpha\ \Delta\delta$, of protomers A and B. It shows a wide range of variation for both the protomers A (0.003-3.6 ppm) and B (0.003-4.0 ppm). SHIFTX2 combines ensemble machine learning methods with sequence alignment-based methods.

Rigidity Analysis

Molecular theorem and protein rigidity

Molecular theorem is the key result used in *pebble game algorithm* to determine the rigidity/flexibility predictions of protein structures by analysing their underlying graphs. For molecular structures, the underlying graph is a simple graph G_M= (V, H_M) where V is the vertex set consisting of bodies of atoms and H_M is the set of molecular hinges around which bodies are free to rotate. Each body is a collection of atoms connected by chemical interactions like double or non-rotatable bonds such that the atoms do not move individually with respect to each other, rather they all move together as a single body. Such bodies of atoms in 3-D have 6 degrees of freedom (three translations and three rotations). Also each hinge between two bodies removes five degrees of freedom (DOF). Replacing bodies with vertices and each hinge with five bars (edges), a body hinge framework becomes a multigraph. Molecular theorem stated below checks the rigidity of multigraph by looking into the rigidity of each of its subgraph.

Theorem (generic): A molecular structure on a graph G_M = (V, H_M) is rigid iff each molecular hinge is replaced by 5 edges, the resulting multigraph G = (V, E) has 6|V| -6 edges and for every non empty set $E' \subseteq$ E with V' vertices, $|E'| \leq 6|V'| - 6$.

Rigidity-based allostery is examined using KINARI software (Fox et al., 2011) that uses pebble game algorithm for classifying the whole protein structure into rigid clusters of different sizes. The distribution of rigid clusters (Figure S4, S6) within protomer A and protomer B indicates the relative flexibility of protomer B. The largest rigid cluster in nitrate bounded protomer A contains total 1684 atoms within the AA residues 30-94 with X_{LRC} = N_{LRC}/N = 0.23 (where N is the total number of atoms in protomer A and N_{LRC} is the total number of atoms in the largest rigid cluster (LRC) in protomer A). This largest cluster involves part of the residues of the neighbourhood of 4.0 A of nitrate binding site and the Thr101 site. To determine fraction of nitrate binding site and Thr 101 site residues in largest rigid cluster in either of the apo and nitrate bound protomers, we calculated

$Z_{LRC}^{A,\,NO_3-unbounded} = 0.24, Z_{LRC}^{A,\,NO_3-bounded} = 0.12\ such\ that\ \Delta Z_{LRC}^{A} = 0.12 > 0\ and\ Z_{LRC\_T101}^{A,\,NO_3-unbounded} = 0.52, Z_{LRC\_T101}^{A,\,NO_3-bounded} = 0.23\ such\ that\ \Delta Z_{LRC\_T101}^{A} = 0.29 >$ **0**.

Positive values of these expressions indicate that nitrate binding is the main source of change in rigidity of protomers **(**Rader and Brown 2010**).** In contrast, there doesn't exits such largest rigid cluster for allostery in protomer B. This theoretical analysis, therefore, suggests that

nitrate-induced conformational changes establish a rigidity-based allosteric communications between the nitrate-binding site and the Thr 101 site that is responsible for priming Thr 101 for phosphorylation.

Mutational Analysis

Noting that most of the new H-bonds in protomer A have been added within the residue range 80-90, AA residues have been chosen from this region for mutational analysis. Nitrate-bound protomer A has been separated from the pdb file (PDB id: 5a2o), repaired in FoldX **(**Schymkowitz et al., 2005**)** to identify and fix bad torsion angles, Vander Waal's clashes so as to complete the structure. This molecule is then taken as input in the UCSF Chimera. Using the mutation tool box (Rotamer), selected single amino acid residue is replaced by the observed or potential residue and then whole protein molecule energy-minimization is carried out in 300 steps with the method of steepest descent minimization to relieve highly unfavourable clashes followed by conjugate gradient minimization. Rigidity-based allosteric analysis has been carried out on this mutated molecule in the KINARI software. Further, the energetic impact of mutations on protein stability is estimated using FoldX, which calculates $\Delta\Delta G$ by using formula $\Delta\Delta G_{fold} = \Delta G_{fold,\ mut} - \Delta G_{fold,\ wt}$. By using method as employed in Studer et al.(2014), we categorized the stabilities of mutants on the basis of their $\Delta\Delta G$ values (Table S5).

To identify key residues in allosteric communication pathway [30-94], all possible *in-silico* mutational analyses have been carried out in protomer A of the NRT1.1 crystallographic structure. This method is calibrated with the experimental results of Ho et al. (2009) in which single amino acid mutants Thr101Asp (T101D) and Thr101Ala (T101A) mimicked as phosphorylated and de-phosphorylated states of NRT1.1, respectively. In parallel to this experimental result, it has been observed that T101A breaks the rigid cluster that is responsible for allosteric communication into two distinct clusters, whereas the T101D retains the intact allosteric rigid cluster. It therefore suggests that priming of T101 site in protomer A for the phosphorylation is allosterically triggered by the high-affinity nitrate-binding, whereas in protomer B such allosteric communication is weak or absent. The analysis showed that Ser 81 is one of the potential key residues for maintaining the allosteric communication pathway. With the mutations of Ser81Thr, Ser81Val, and Ser81Asp, the allosteric rigid-cluster splits into two distinct clusters due to the loss of H-bonds between Ser 81 and Phe 77, and Ser 81 and Cys 85 which were added through nitrate-binding.

Supplemental references

Fox, N., Jagodzinski, F., Li, Y., and Streinu, I. (2011). KINARI-Web: A server for protein rigidity analysis. *Nucleic Acids Research* 39, 177–183.

Humphrey, W., Dalke, A., and Schulten, K. (1996).VMD - Visual Molecular Dynamics. *Journal of Molecular Graphics* 14, 33-38.

Jones, T.A., Zou, J.Y., Cowan, S.W., and Kjeldgaard, M. (1991). Improved methods for building models in electron density maps and the location of errors in these models. *Acta Crystallographica Section A* 47, 110–119.

Pettersen, E.F., Goddard, T.D., Huang, C.C., Couch, G.S., Greenblatt, D.M., Meng, E.C., and Ferrin, T.E.(2004) UCSF Chimera - a visualization system for exploratory research and analysis. *Journal of Computational Chemistry* 25, 1605-1612.

Ramachandran, G. N., Ramakrishnan, C., and Sasisekharan, V. (1963). Stereochemistry of polypeptide protomer configurations. *Journal of Molecular Biology* 7, 95–99.

Schymkowitz, J., Borg, J., Stricher, F., Nys, R., Rousseau, F., and Serrano, L. (2005). The FoldX web server: an online force field. *Nucleic Acids Research* 33, 382 – 388.

Studer, R.A., Christin, P.A., Williams, M.A., Orengo, C.A. (2014). Stability-activity tradeoffs constrain the adaptive evolution of RubisCO. *Proc. Nat. Acad. Sc. (USA)* 111, 2223–2228.

Winn, M.D., Ballard, C.C., Cowtan, K.D., Dodson, E.J., Emsley, P., Evans, P.R., Keegan, R.M., Krissinel, E.B., Leslie, A.G., McCoy, A., McNicholas, S.J., Murshudov, G.N., Pannu, N.S., Potterton, E.A., Powell, H.R., Read, R.J., Vagin, A., and Wilson, K.S. (2011). Overview of the CCP4 suite and current developments. *Acta Crystallographica Section D* 67, 235–242.